Enhanced Southern Ocean biomass with increased Diapycnal mixing

Key Points:

- The rate of modelled vertical mixing is a key control on Southern Ocean biomass over annual timescales
- Increased mixing enhances diapycnal fluxes of nutrients to surface waters which increases biomass

Abstract

The Southern Ocean (SO) is the worlds largest high nutrient low chlorophyll region, and has a plentiful supply of underutilised macronutrients due to light and iron limitation. These macronutrients supply the rest of the neighboring ocean basins, and are hugely important for global productivity and ocean carbon sequestration. Vertical mixing rates in the SO are known to vary by an order of magnitude temporally and spatially, however there is great uncertainty in the parameterization of this mixing, including in the specification of a background value in coarse resolutation Earth System Models. Using a biogeochemical-ocean model we show that SO biomass is highly sensitive to altering the background diapycnal mixing over short timescales. Increasing mixing enhances biomass by altering key biogeochemical and physical parameters. An increased surface supply of iron is responsible for biomass increases in most areas, demonstrating the importance of year round diapycnal fluxes of iron to SO surface waters. These changes to SO biomass could potentially alter atmospheric CO_2 concentration over longer timescales, alluding to the importance of accurate representation diapycnal mixing in climate models.

Plain Language Summary

[enter your Plain Language Summary here or delete this section]

1 Introduction

Phytoplanktons are photosynthesising organisms, able to use energy from the sun to convert dissolved inorganic carbon to organic carbon. Phytoplankton are responsible for around 50% of Earth's primary productivity. The Southern Ocean (SO) has a key role in global biological production (Sigman et al., 2010; Gruber et al., 2009; Takahashi et al., 2009). Strong westerly winds cause the upwelling of nutrient and carbon rich deep waters to the ocean surface, resulting in high macronutrient concentrations, including of phosphate and nitrate. Nutrient utilisation in the SO is limited, primarily due to micronutrients (especially iron, Fe) (P. W. Boyd, 2002) and light (Fauchereau et al., 2011) limitation preventing phytoplankton growth and reproduction. The SO is therefore classified as a high nutrient low chlorophyll (HNLC) zone.

The underutilised SO macronutrients go on to fertilize nutrient depleted surface waters in the neighboring ocean basins to the north (Parekh et al., 2005; Dutkiewicz et al., 2005), accounting for up to 75% of primary production north of 30°S (Palter et al., 2010). This makes SO nutrient upwelling and under utilisation a key control on phytoplankton production throughout the global ocean (Sarmiento et al., 2004). Phytoplankton are also essential in the biological carbon pump (BCP), the mechanism which maintains 90% of the vertical gradients of dissolved inorganic carbon in the ocean (Longhurst, 1991). The BCP is a key control on ocean carbon sequestration, meaning it's strength and efficiency have a strong effect on atmospheric CO_2 levels (Ito & Follows, 2005).

The background value of cross-density (diapycnal) mixing in the ocean interior due to breaking internal waves is subject to debate. Since the seminal work of Munk, bulk measures of mixing have found $K_v \sim \mathcal{O}(10^{-4})$ m^2 s^{-1} is required to close the upwelling branch of the meridional overturning circulation (Ganachaud & Wunsch, 2000; Talley et al., 2003; Lumpkin & Speer, 2007; Talley, 2013), whereas estimates from profiling instruments often find $K_v \sim \mathcal{O}(10^{-5})$ m^2 s^{-1} in the ocean interior and much larger values only close to the seafloor (Waterhouse et al., 2014). Models are not able to resolve these small scale mixing processes, relying on parameterisations. While the precise value of this background mixing impacts hydrography and circulation on climate timescales (Schmittner et al., 2005), altered values appear to have a strong effect on the distribution of biogeochemical tracers over shorter timescales (Gnanadesikan et al., 2004; Garabato et al., 2007; Cimoli et al., 2017).

Diapycnal mixing rates play a role in setting SO water temperatures, stratification, and the mixed layer depth (MLD), which all alter light availability and the supply of nutrients (Fauchereau et al., 2011; Swart et al., 2015), as well as altering the diapycnal flux of nutrients themselves. For example, topography induced mixing around seamounts in the SO has been observed to increase productivity via increased nutrient supply from diapycnal mixing as well as from possible isopyncal doming within eddies (von Berg et al., 2020).

There is uncertainty over whether light or Fe predominately limit phytoplankton productivity, and seasonal cycles in biomass are dominated by the interactions between light and nutrient (Fe) availability. The MLD controls the depth from which nutrients are supplied (P. W. Boyd et al., 2008), and levels of light limitation. A deepening of the MLD can therefore cause an increase in nutrient supply, but a decrease in light supply (Fauchereau et al., 2011). Light availability also depends on incoming irradiance and self shielding from phytoplankton biomass. Major processes supplying surface waters with Fe are the entrainment of Fe rich waters in the deep winter mixed layers, diapycnal mixing (especially during storms) (Llort et al., 2019; Tagliabue et al., 2014), and Ekman upwelling / downwelling (Tagliabue et al., 2014). Winter entrainment pulses can supply more Fe than diapycnal diffusion, as the ferrocline occurs at depths below that of the MLD (Tagliabue et al., 2014), meaning surface Fe concentrations are believed to be set more by the winter MLD than the summer MLD (P. W. e. a. Boyd, 2000). The range of physical and biogeochemical phytoplankton growth factors affected by altered SO diapycnal mixing makes it hard to predict how SO productivity will be changed.

In this work we use an eddy permitting ocean state estimate that includes a biogeochemical cycle and assimilates a host of in-situ and remote sensing data (Verdy & Mazloff, 2017) to explain the biologically significant changes to Fe, NO_3, light availability, and surface temperatures observed with increased diapycnal mixing. We are able to show that SO biological productivity is highly sensitive to altered mixing, with strong regional and seasonal variations in this sensitivity. The increase in surface Fe supply via diapycnal fluxes is the dominant factor in the observed increase to biological productivity with enhanced mixing.

2 Model Description

The biogeochemical Southern Ocean state estimate (B-SOSE) used here is a data-assimilating state estimate with a resolution of $1/6^\circ$ and 52 vertical layers, physics based on the MITgcm, and the NBLING biogeochemical model, as described fully in (Verdy & Mazloff, 2017). B-SOSE assimilates SOCATv5 and Argo data, including biogeochemical parameters from the SOCCOM float array, providing a baseline estimate of the ocean state that is dynamically consistent. The full set of model parameters used in this $1/6^\circ$ set up are given in (Swierczek et al., 2021). A vertical diffusivity is employed with values discussed in the next paragraph, and a lateral biharmonic diffusivity is used with a value of 10^{-8} $\mathrm{m^4 s^{-1}}$. The GGL90 mixed layer parameterization of Gaspar, Grégoris, and Lefevre is used, as is an implicit vertical diffusivity for convection of 10 $\mathrm{m^2 s^{-1}}$. No mesoscale eddy parameterization is implemented.

For the purpose of our work, from the model output he mixed layer depth is calculated based on the first and second derivatives of density. For any point where the water column is deeper than 3 grid cells, the depth of the maximum vertical density gradient is found. Above this the maximum second derivative of density with depth is used to find where the stratification is increasing the fastest above the pycnocline. This point is defined as the MLD .

The biogeochemical state is simulated using a modified Biogeochemistry with Light, Fe, Nutrient, and Gases (BLING) model (Verdy & Mazloff, 2017; Galbraith et al., 2010) which includes nine prognostic tracers (alkalinity, dissolved inorganic carbon [DIC], inorganic and

organic nitrogen and phosphorus, Fe, oxygen, and biomass). The biomass is partitioned into three phytoplankton groups (small, large, and diazotrophs). Biological activity is influenced by light, NO_3, PO_4, Fe availability, and temperature, and influences carbon and oxygen concentrations.

Within the NBLING model, biological productivity is parameterised. The light saturated maximal photosynthesis rate term (pc_m), is the product of the prescribed maximum photosynthesis rate (pc_0), the Epply temperature dependence, and a co-limitation term which is the product of Michaelis-menten nitrate(NO_3) limitation, phosphate(PO_4) limitation or iron (Fe) limitation:

$$pc_m = pc_0 \times e^{\kappa_T} \times min(\frac{NO_3}{\kappa_{NO_3} + NO_3}, \frac{PO_4}{\kappa_{PO_4} + PO_4}, \frac{Fe}{\kappa_{Fe} + Fe}. \tag{1}$$

Therefore pc_m is sensitive to temperature and nutrient concentrations, varying amplitudes based on κ_T, κ_{NO_3}, κ_{NO_3}, κ_{NO_3}.

The nitrate, phosphate, iron and light limitation terms

$$\frac{NO_3}{\kappa_{NO_3} + NO_3}, \frac{PO_4}{\kappa_{PO_4} + PO_4}, \frac{Fe_d}{\kappa_{Fe} + Fe_d}, 1 - e^{-irr_{inst}/irr_\kappa} \tag{2}$$

all vary between 0 and 1, with a value near 1 meaning there is high availability of that nutrient (or light) at that time and space, while a value near 0 will mean that phytoplankton growth is severely limited by that nutrient (or light). irr_{inst} is the instantaneous irradience field and irr_K is the nutrient limited efficiency of algal photo systems. When short wave radiation hits the ocean, it is attenuated as a function of chlorophyll concentration, based on works of Manizza, Quéré, Watson, and Buitenhuis. Denser chlorophyll results in more light attenuation, a process referred to as shelf shielding.

The carbon specific photosynthetic rate is given as

$$\mu = pc_m(1 - e^{-irr_{inst}/irr_\kappa}), \tag{3}$$

This term accounts for the sensitivity of phytoplankton growth to light availability and nutrient concentrations.

3 Experiment Design

Two model simulations were carried out, each with a different constant background diffusivity value added to the GGL90 parameterized mixing. Ex1e-5 has a background diffusivity value of $10^{-5} m^2 s^{-1}$, whilst Ex1e-4 has a background value of $10^{-4} m^2 s^{-1}$, which prior to this work was the default value used in B-SOSE for optimization (Verdy & Mazloff, 2017). The range 10^{-5} $m^2 s^{-1}$ to 10^{-4} $m^2 s^{-1}$ is a conservative range, representing the two canonical paradigms of mixing in physical oceanography (Ferrari, 2014). For example, in the Diapycnal and Isopycnal Mixing Experiment in the Southern Ocean (DIMES), estimates of mixing based on microstructure profiles reported $K_v \sim \mathcal{O}(10^{-5})$ m^2 s^{-1} at the mean depth of an anthropogenic tracer released upstream of the Drake Passage but the tracer itself seemed to experience $K_v \sim \mathcal{O}(10^{-4})$ m^2 s^{-1} (Watson et al., 2013; Mashayek et al., 2017). Examining regional and seasonal trends and changes in biological productivity between these two experiments allows us to understand how altered mixing may alter biological productivity in the Southern Ocean over relatively short times scales.

4 Results

4.1 Southern Ocean Biomass

The water column intergrated biomass produced by B-SOSE shows spatial and temporal variation, due to variations in light, nutrients and temperature (Fig.1a&b). The annual

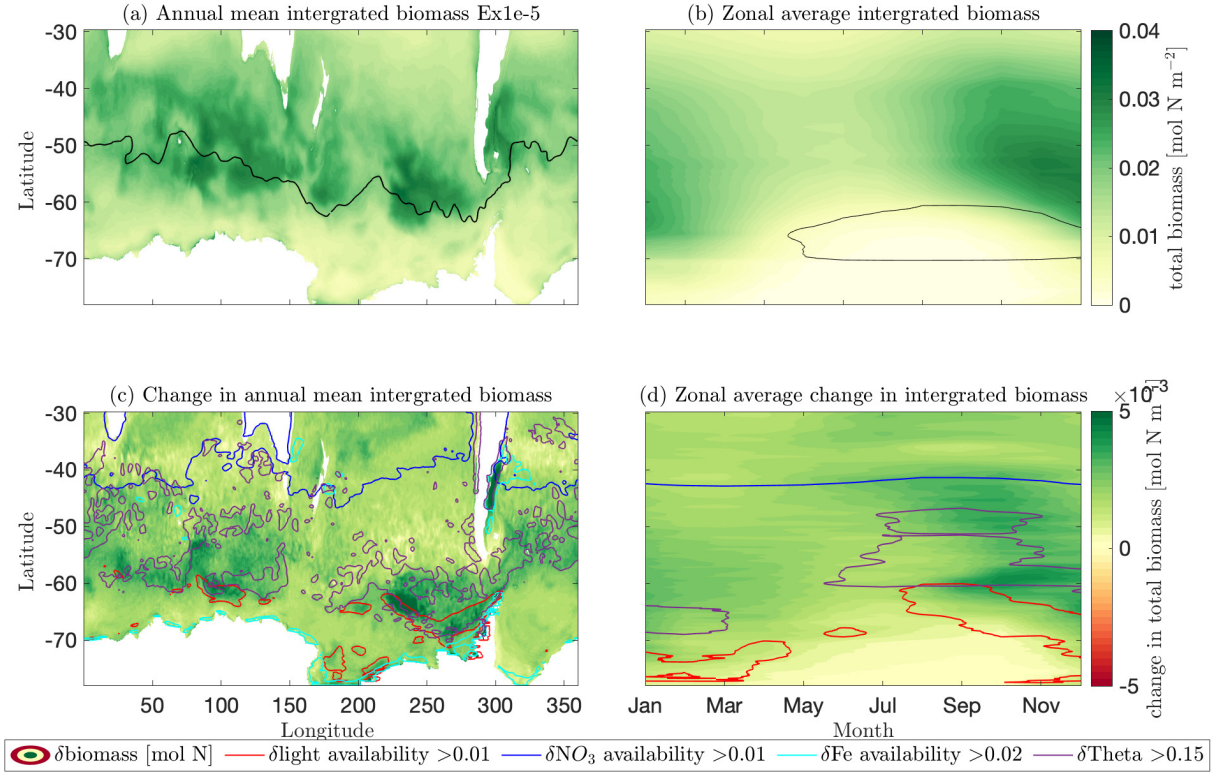

Figure 1. a) Annual mean intergrated biomass in Ex1e-5 (2013-2018). SO polar front (pf) shown by the black line. b) Seasonal cycle of zonal average intergrated biomass. Seasonal cycle of average sea ice extent shown by the black line. c) Change (Ex1e-4 - Ex1e-5) in annual mean intergrated biomass (2013-2018) d) Change (Ex1e-4 - Ex1e-5) in zonal average intergrated biomass over a seasonal cycle. Colored contours indicate where light availability (red), NO_3 availability (dark blue) and Fe availability (light blue) are increased and temperature (purple) is increased in Ex1e-4 compared to Ex1e5

mean intergrated total water column biomass (Fig.1a) is greatest at latitudes around 55°S, following the polar front (PF), with high biomass also found in the Argentine basin. These are both regions characterized by strong upwelling. Annual mean biomass south of the PF is low due to the seasonal ice cover, low temperatures and low light availability. North of 40°S the biomass is also fairly low due to nutrient limitation, mainly of NO_3.

Productivity and biomass show strong seasonal patterns shown in fig.1b. In January, the highest biomass is found at lower latitudes of around 60°S, with fairly high biomass found up as far north as 40°S. Throughout autumn, the biomass at all latitudes gradually decreases, as temperatures and light decrease. The latitude of the maximum biomass shifts further north into the winter. As ice cover extends northward throughout winter, a greater region of the south becomes ice covered where biomass is very low. The lowest average intergrated biomass occurs in June when light is at most limiting. Biomass increases again in August as spring begins and light and temperatures once again increase, combined with a rich nutrient supply from wintertime deep water entrainment and mixing. Throughout spring the latitude of maximum productivity shifts further south again, where nutrients are less limiting. Dec and Jan have the highest average intergrated biomass over all latitudes.

4.2 Changes in biomass

Changes in biomass are seen with altered mixing, and are directly proportional to changes in net community productivity (Fig.1c,d). These changes are observable in the first month, when biomass increases by over 3% in Ex1e-4 in all regions at all times of year. In the second year of the experiment, the mean annual increase in intergrated biomass is 20%, with a mean increase of 29% seen over this 5 year period at latitudes south of 60°S. Changes in biomass show strong spatial and seasonal variations in the difference between the two model runs (Fig.1c,d). December has the greatest mean increase in biomass over all latitudes (2.4e-3 mol N m^{-2}) with an increase of 15%, while July has the lowest mean increase (1.2e-3 mol N m^{-2}), though due to low biomass in July this actually represents the largest percentage increase (28%). The strongest zonal average differences between experiments is 4.7e-3 mol N m^{-2}, at 59°S in November.

Colored contours of fig.1 c,d show regions where the phytoplankton light availability (red), NO_3(blue) and Fe (light blue) availability are increased with stronger diapycnal mixing in Ex1e-4, and where the water temperature (purple) is increased. The contour intervals shown for changes in Fe availability are 0.2, while NO_3 nutrient availability change contour intervals are 0.1. Surface Fe availability increases by 0.1 over vast areas of the SO (not shown). Contours for changes in PO_4 availability are not shown, as no regions of the SO are PO_4 limited in either experiment. Temperature change contours shown are for 0.15 °C.

Regions with the greatest increase in biomass in Ex1e-4 include the Argentine basin, where Fe availability is strongly increased, Fe availability is also increased along the coast of Antarctica. In Ex1e-4, the greatest increase in biomass over the 6 year period of the experiment is around latitudes of 59°S. This latitude roughly corresponds to a region of increased water temperature and light availability in Ex1e-4. Productivity also increases around 30°S in the Pacific and Indian basins, corresponding to areas of enhanced NO_3.

The changes in light availability are also only present during the spring months, and are found at latitudes from 60- 70°S. Changes in NO_3 availability are concentrated in the northern SO, and occur over all months of the year. Strong seasonal changes to Fe availability are not visible when examined in a zonal average sense. Increases to surface water temperatures occur from winter to later summer. The increased temperatures are far more widespread and extend to higher latitudes during the spring months. Changes to temperatures are confined to the southern latitudes during late spring and summer.

Through this paper we describe how the biomass changes are attributed to changes to light, Fe and NO_3 availability, and temperature as a result of enhanced diapycnal mixing.

4.3 Changes in Nutrient availability

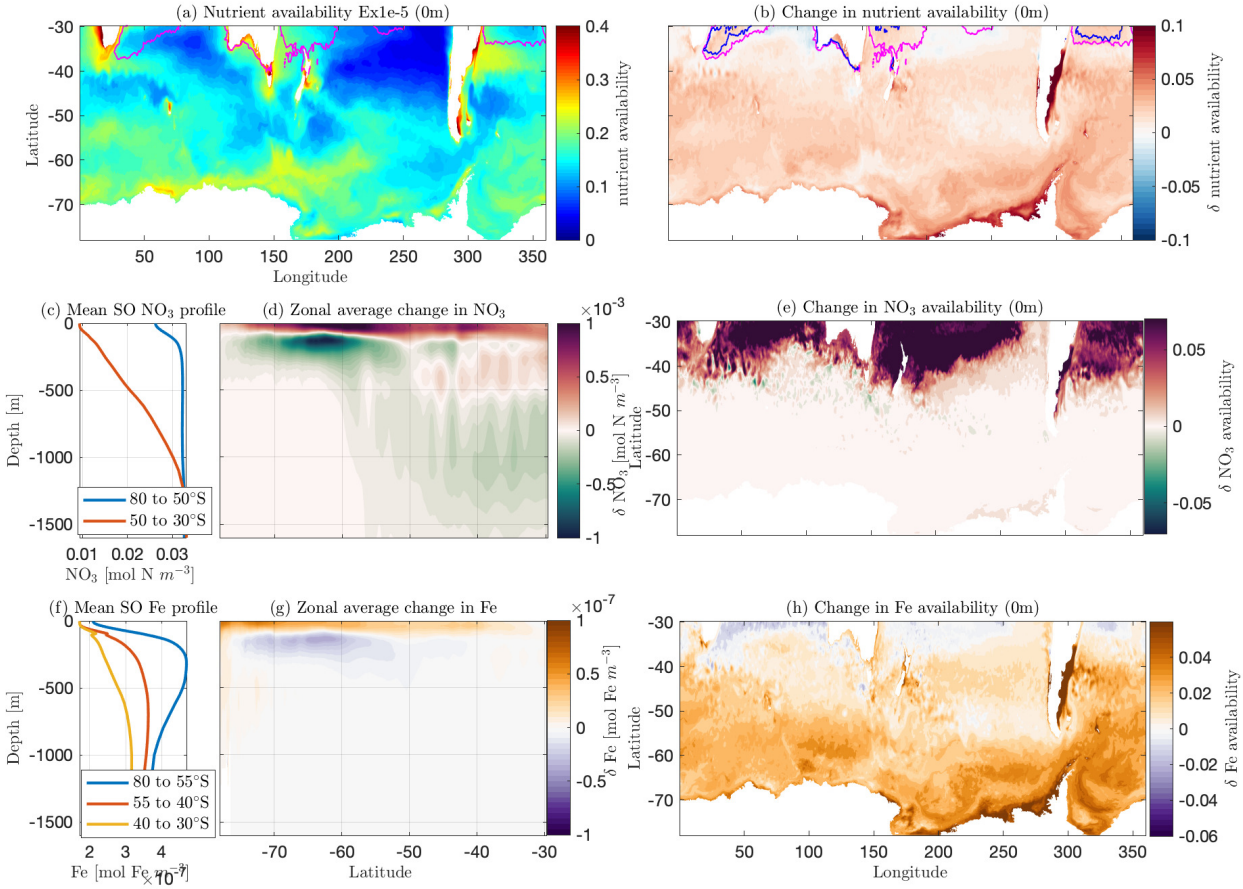

Figure 2. a) Annual mean surface nutrient availability ($min(Fe_{lim}, No_{3lim}, PO_{4lim})$) of Ex1e-5. Pink line surrounds region of NO_3 limitation, all other regions are Fe limited. b) Annual mean change in nutrient availability (Ex1e-4 - Ex1e-5). Pink line shows region of NO_3 limitation for Ex1e-5, blue line shows region of NO_3 lim in Ex1e-4. c) Annual mean zonal average NO_3 profile from 80°S to 50°S (blue line) and from 50°S to 30°S (red line). d) Zonal average annual mean change in NO_3 concentration (Ex1e-4 - Ex1e-5). e) Annual mean change in surface NO_3 availability (Ex1e-4 - Ex1e-5). f) Annual mean zonal average Fe profile from 80°S to 55°S (blue line), 55°S to 40°S (orange line) and from 40°S to 30°S (yellow line). g) Zonal average annual mean change in Fe concentration (Ex1e-4 - Ex1e-5). h) Annual mean change in surface Fe availability (Ex1e-4 - Ex1e-5).

Phytoplankton nutrient limitation is set by the co-limiting term, which is set by the concentration of the nutrients following Equation 2. The phytoplankton of the SO are strongly nutrient limited, with significant regional variations (Fig.2a). A value close to 0 represents low nutrient availability and strong limitation. The regions with the lowest nutrient availability include the northern Pacific and Indian ocean. Regions with higher nutrient availability tend to be closer to land masses, including the Argentine basin, the south coast of Australia, off the western tip of Africa and along the Antarctic continent. In general, the waters further north have lower nutrient availability than waters further

south. In this model, for almost all of the SO; Fe is the limiting nutrient. NO_3 is the limiting nutrient in small regions of the northern SO, NO_3 limited regions are outlined in pink (Fig.2a). As previously mentioned, no region of the SO is found to be PO_4 limited.

Surface waters have lower nutrient availability compared to subsurface waters due to biological depletion (Fig.2c,f). NO_3 concentrations increase with depth throughout the SO, with deep waters enriched in NO_3 due to the respiration of organic material and the release of NO_3 (Williams & Follows, 2011). North of 60°S, the nitracline of NO_3 is much deeper than in the south, and the concentration gradients are less steep (Fig.2c). Fe concentration increases with depth down to a subsurface maxima at around 450m, below this depth they then become further depleted, due to scavenging and precipitation due to the low solubility of Fe (Fig.2f) (Lefèvre & Watson, 1999). The subsurface waters with higher concentrations of nutrients are therefore less nutrient limited, however these waters experience severe light limitation.

SO nutrient distributions and phytoplankton nutrient availability are both altered from Ex1e-5 to Ex1e-4. Nutrient availability in surface waters across the SO increases with increased diapycnal mixing (Fig.2b), with the only exception being slight decreases in availability in the very north of the Indian ocean. Regions with the greatest increase in nutrient availability include the Argentine basin and the coast of Antarctica. The region with NO_3 rather than Fe limitation are also reduced in Ex1e-4 (blue vs pink lines), meaning Fe is the limiting nutrient over an even great area in Ex1e-4 than in Ex1e-5.

The concentrations of Fe and NO_3 through the water column is altered between the two experiments (Fig.2d,g). The diapycnal flux for a tracer is given by

$$-K_v \times \frac{\delta tracer}{\delta z}$$

where K_v is the diapycnal diffusivity rate and $\frac{\delta tracer}{\delta z}$ is the vertical tracer gradient. Therefore, the diapycnal flux of a tracer is proportional to the strengths of the vertical tracer gradient and the effective diapycnal mixing. An increase in diapycnal mixing causes more tracer to mix down gradient from high to low concentrations. This results in an increased upward flux of surface depleted nutrients with higher mixing rates, hence an enhanced surface nutrient concentration in Ex1e-4. The increased upward flux with increased diapycnal mixing below the depth of the maximum vertical nutrient gradient is less than the increased upward flux at the depth of maximum gradient. Therefore, below the depth of the maximum vertical gradient, nutrient concentrations are reduced in Ex1e-4 due to a flux divergence.

The concentration changes in NO_3 show more latitudinal variations than changes to Fe concentration. South of 50°S, NO_3 concentration increases in waters above approximately 75 m while subsurface water NO_3 concentration decrease. The strongest changes occur around 64°S, where vertical gradients are the strongest. In the north, the deeper nutracline and less steep vertical gradients cause NO_3 concentrations to increase above depths of around 500 m and decrease below, with the strongest increases occurring in the surface waters.

The concentration of Fe increases with a higher mixing value in waters above depths of around 85 m meters (where the vertical gradient of Fe is the strongest), and decreases below 100 m, from 75°S to around 45°S. Further north of 45°S, surface waters still increase in Fe concentration, but to a lesser extent than in the very south, and subsurface waters do not experience such a strong reduction in Fe concentration. This is due to weaker vertical gradients in Fe concentration occurring in waters further north.

The changes to nutrient concentrations cause changes to Fe and NO_3 availability (Fig.2e,h). Almost all surface waters of the SO have increased Fe availability in Ex1e-4 due to increased Fe concentration. Very strong increases occur in the Argentine basin, off the coast of Antarctica, and in waters south of 60°S. Surface waters from around 55°S to 45°S show very slightly increased Fe availability. In areas where Fe is the most limiting nutrient, an increase in Fe availability results in increased phytoplankton productivity and

biomass. Surface waters have decreased Fe availability in the very north, especially in the Indian ocean. However, Fe is not the limiting nutrient in these areas, so the co-limiting term term remains unchanged. Increases to surface NO_3 availability in Ex1e-4 are only seen in the very north, as in the the more southerly waters, NO_3 availability is already high, hence the extra NO_3 fluxed up into the surface waters made no changes to the NO_3 availability. Therefore, changes in NO_3 availability do not resemble the redistribution of NO_3.

4.4 Changes in mixed layer depth and temperature

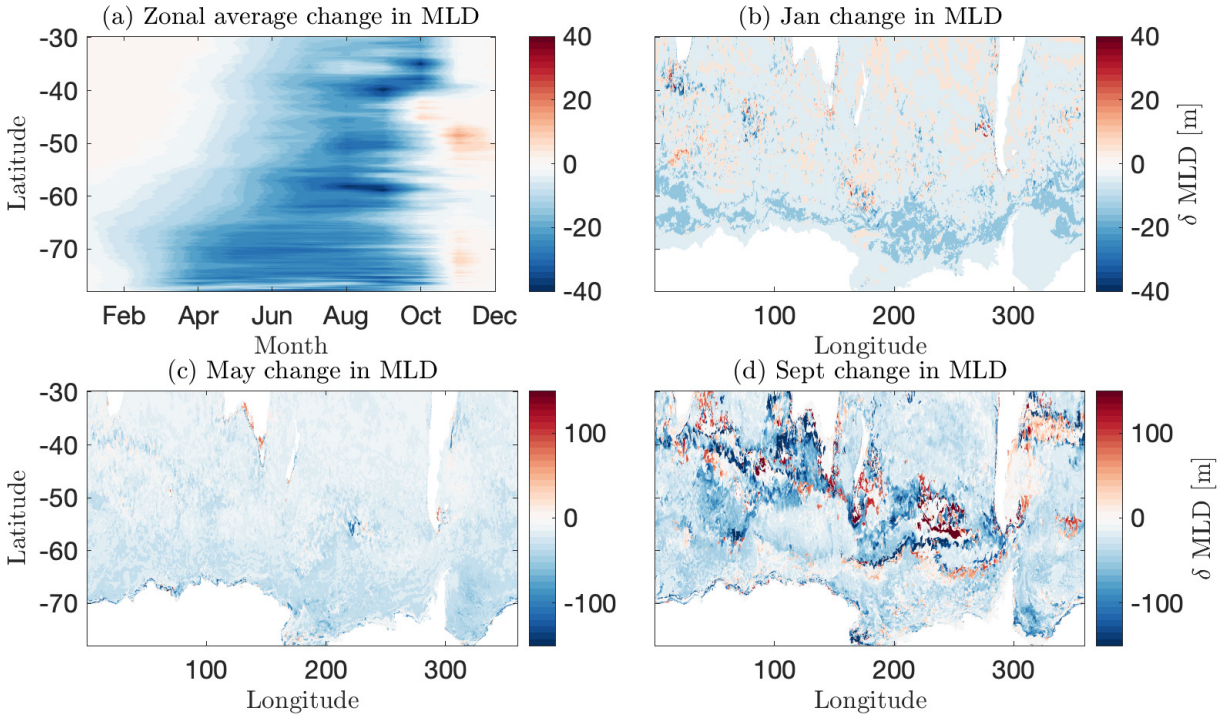

Figure 3. a) a) Seasonal cycle of zonal average change in mixed layer depth (MLD) (Ex1e-4 - Ex1e-5). b) January change in MLD (Ex1e-4 - Ex1e-5). c) May change in MLD (Ex1e-4 - Ex1e-5). d) September change in MLD (Ex1e-4 - Ex1e-5). Note the different color scale used for September and May.

The mixed layer depth is generally deepened with increased SO diapycnal mixing (Fig.3). Changes vary seasonally and with latitude, with changes in the summer being the smallest (Fig.3a; note the different color scales used in Fig.3). In the summer (January), while a slight deepening (more negative value) of the MLD occurs around 70°S, a shallowing of the MLD occurs north of 50°S (Fig.3b). In May, there is deepening of the mixed layer everywhere in Ex1e-4, except off the south coast of Australia, where the MLD becomes shallower (Fig.3c). The greatest changes in MLD occur in the late winter, where the MLD deepens in Ex1e-4 by almost 300 m in some areas (Fig.3d). The MLD also shoals around the ice front.

The increased mixing of Ex1e-4 results in a deepened MLD, especially in the winter over storm tracks. Climatological MLDs are known to mirror pynocline stratification (Sallée et al., 2021). As the higher mixing of Ex1e-4 is able to erode the density gradients, storm track induced turbulence is better able to penetrate through, deepening the MLD. The weak vertical stratification found in the water column in winter means that an increase in

diapycnal mixing can result in the breakdown of this stratification and a deepening of the MLD.

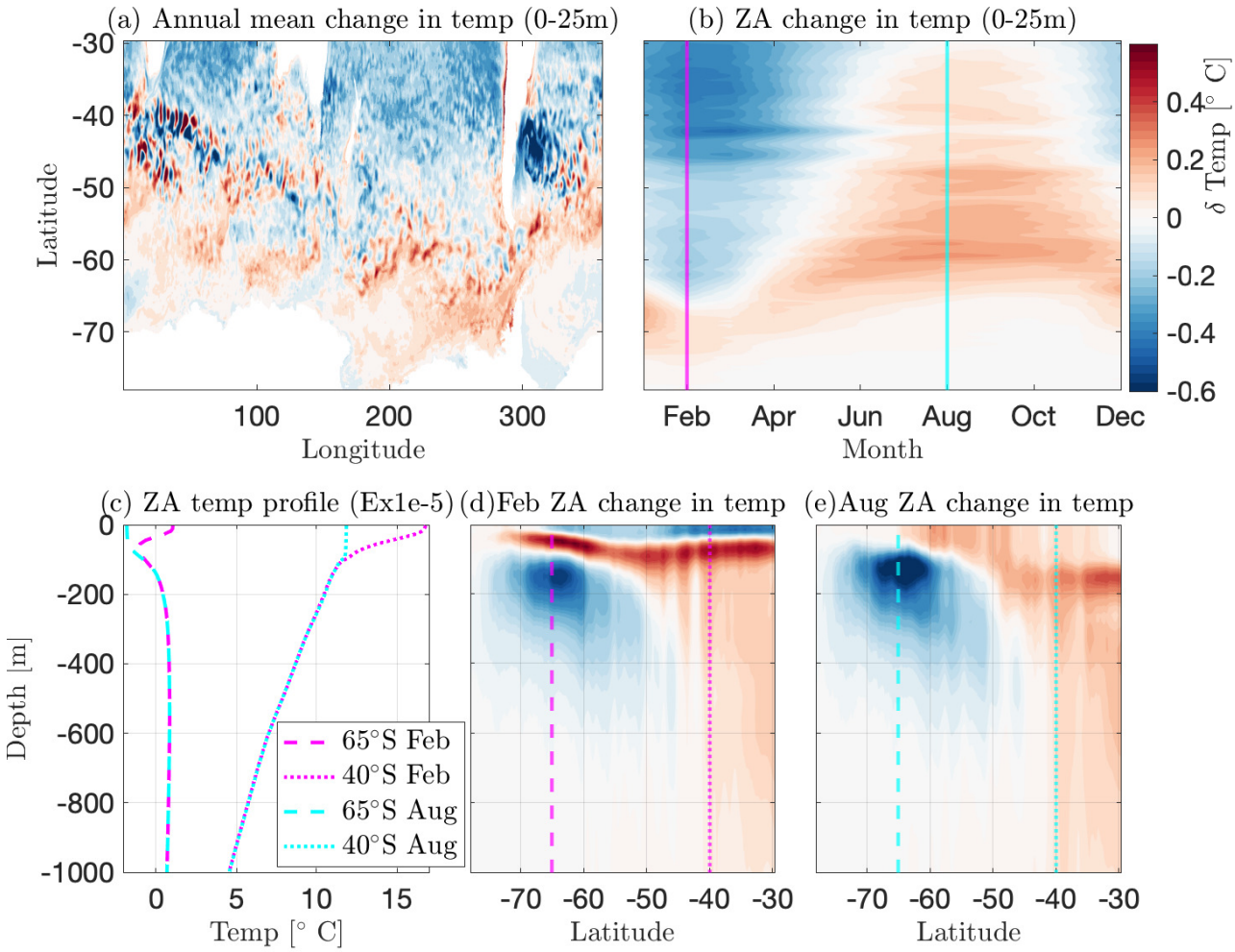

Figure 4. a) Annual mean change in temperature averaged over 0 m to 25 m (Ex1e-4 - Ex1e-5). b) Seasonal cycle of zonal average change in temperature averaged over 0 m to 25 m (Ex1e-4 - Ex1e-5). c) Zonal average temperature profile at 65°S (dashed) and 40°S (dotted) for Feb (pink) and August (blue) for Ex1e-5. d) February zonal average change in temperature (Ex1e-4 - Ex1e-5). e) August zonal average change in temperature (Ex1e-4 - Ex1e-5).

Altered mixing also causes changes to the surface temperature of the SO (Fig.4). Annual mean surface temperatures generally increase south of the Polar Front in Ex1e-4, whilst further to the north, temperatures of the surface waters generally decrease with increased diapycnal mixing (Fig.4.a). The strongest changes to surface temperatures occur in the Argentine basin, where temperatures are strongly decreased in Ex1e-4. The latitudinal and seasonal variation in the effect of increased mixing is due to the difference in the vertical structure of the thermocline at different latitudes (Fig.4).

In the summer months most latitudes decrease in surface temperatures with enhanced mixing (Fig.4.b,d). Incoming solar radiation during the summer results in warmed surface

waters, and induces strong vertical gradients in temperature in the upper 100m of the water column (Fig.4.c pink lines). Temperatures decrease with depth throughout the water column (Fig.4.b, c, d). Enhanced mixing results in more heat being mixed down from the surface, cooling surface waters and warming those around 70 m. Therefore, strong surface cooling and subsurface warming occurs at almost all latitudes.

South of around 65°S, temperatures decrease with depth down to around 70 m, where a temperature minimum occurs; below this temperatures increase with depth. Here surface temperatures are increased with enhanced diapycnal mixing, with more heat being upwelled from the deep into the temperature minimum at 70 m.

In the winter the upper 100 m of the water column is well mixed due to winter storms leading to wind induced mixing (Fig.4.b, c, e). South of 65°S, surface waters of the mixed layer are cooled by the atmosphere, and below the mixed layer, water temperatures increase with depth. Therefore, increased mixing mixes more heat into the surface layers. At lower latitudes, the temperature decreases with depth below the MLD, as surface waters are warmed by solar radiation. An increase in the temperature of the entire water column in Ex1e-4 is due to the increased downward mixing of heat.

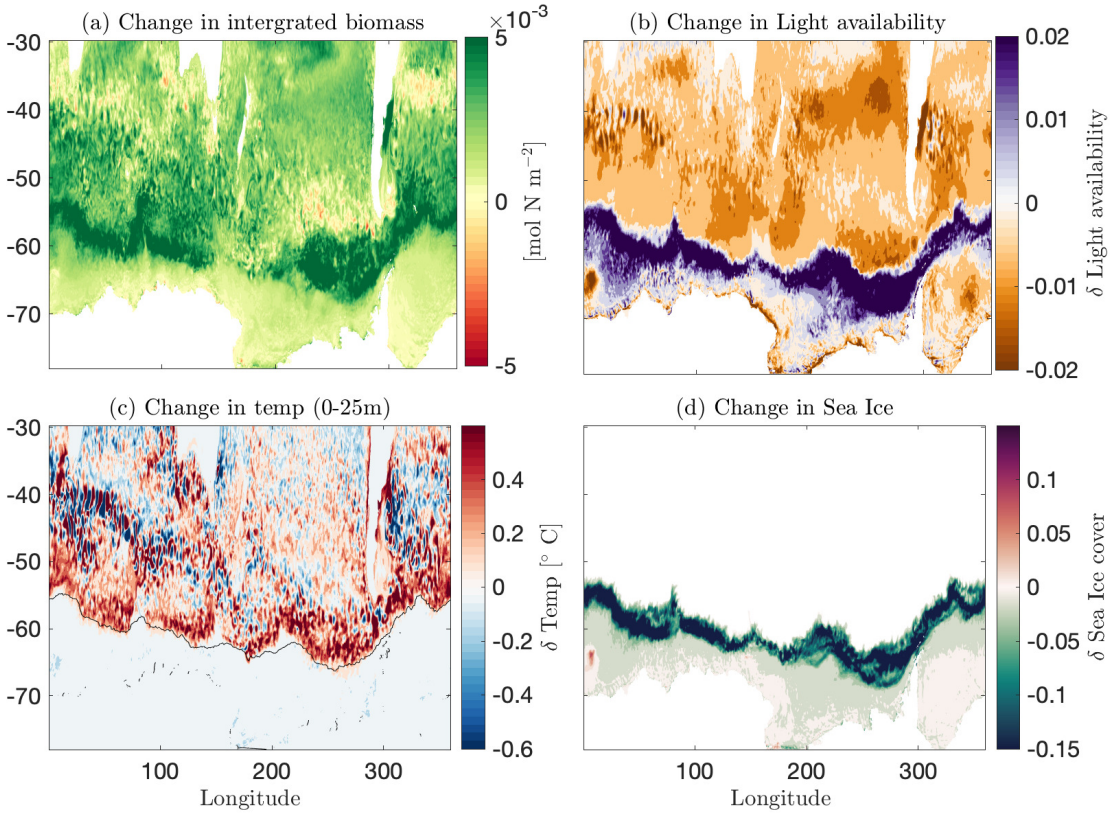

Figure 5. a) Change in intergrated biomass for September(Ex1e-4 -Ex1e-5). b) Change in light availability for September(Ex1e-4 -Ex1e-5). c) Change in temperature averaged over 0m to 25m for September(Ex1e-4 -Ex1e-5). d) Change in sea ice cover for September(Ex1e-4 -Ex1e-5).

A strong seasonal increase in biomass occurs in Ex1e-4 in a thin band towards the south, around latitudes of 55°S (Fig.5a). Sea ice extends over vast regions of the SO during winter, but melts during the spring as air and surface water temperatures increase. The

surface waters around the ice sheet edge in Ex1e-4 are warmer (Fig.4, Fig.5 c), increasing the rate of the spring ice sheet melt. Therefore, ice cover in Ex1e-4 is reduced (Fig.5 d), and the light availability increases, as sea ice has a high albedo preventing light from entering the ocean (Fig.5 b). The edge of the springtime ice sheet becomes a region with highly increased light availability in Ex1e-4.

In the rest of the ocean (in all seasons), light availability is reduced from Ex1e-5. This is due to higher biomass increasing the attenuation of incoming solar radiation through the water column, reducing light availability via self shielding mechanisms, and due to deeper MLDs. The region with the strongest reduction in light availability include the Argentine basin, a region with one of the strongest increases in biomass. The sea ice melt can also result in increased vertical stratification, reducing the mixed layer depth thereby further increasing light availability.

5 Discussion

In summary, increased diapycnal mixing in the SO causes a strong and widespread increase in SO biomass in all seasons. Though altered diapycnal mixing changes both physical and biogeochemical factors, with the exception of the ice front during spring, it is the changes to nutrient supply which dominate the changes to phytoplankton biomass.

The depth and properties of the MLD strongly influence the availability of light and nutrients for phytoplankton growth (Sallée et al., 2010). The decreased light availability seen in Ex1e-4 is likely due to a combination of increased attenuation of light from shelf shading due to increased biomass, as well as the deepening of the MLD. Deepening of the deep SO winter MLD may have little impact on phytoplankton biomass as strong light limitation is already occurring(Sallée et al., 2010). Strong light limitation is also highly seasonal in the HNLC SO (Venables & Moore, 2010). Together this makes biomass less sensitive to changes in light availability throughout the year. The dominant changes seen with enhanced mixing are due increased nutrient concentrations.

An increased supply of Fe into the upper 75 m of the water column is the leading cause of increased biomass across most of the SO when mixing is enhanced. There are many observations of phytoplankton blooms in the SO in regions with large Fe inputs, such as seasonal ice zones, in shallow coastal waters, and within the ACC upwelling fronts. Ocean fertilisation experiments have also conclusively demonstrated that increased Fe supply is able to increase biological productivity in such regions (Yoon et al., 2018). In the northern SO, it is the increase in surface nitrate supply that increased productivity. The increased surface water temperatures during the winter months, when background temperatures are at the lowest, also contributed to the increased rate of productivity due to the Eppley temperature dependence of pc_m.

Given that surface Fe concentrations are believed to be set more by the winter MLD, we could expect that the deeper winter MLDs observed with enhanced mixing would have increased the winter replenishment of surface waters with Fe. However, subsurface waters become depleted in nutrients in Ex1e-4 relative to Ex1e-5 due to an increased upward diapycnal flux. The subsurface depletion depth corresponds to the depths of the mixed layer (Fig.6c). Therefore, the combination of the two effects, the deepened mixed layer, and depleted subsurface nutrient concentration result in no net change in Fe concentration at the base of the MLD from Ex1e-4 to Ex1e-5, especially during winter (Fig.6d). This suggests that a deeper winter MLD in Ex1e-4, and therefore stronger winter Fe entrainment are not the dominant causes of the increase in surface Fe in Ex1e-4. The increased background diapycnal mixing and diapycnal flux of Fe is responsible for increasing Fe availability.

While altered nutrient supply dominate changes to phytoplankton biomass in most of the SO, temperature, ice cover and light availability changes dominate changes to phytoplankton along the ice sheet edge during spring. Reduced sea ice, as seen in spring in Ex1e-4

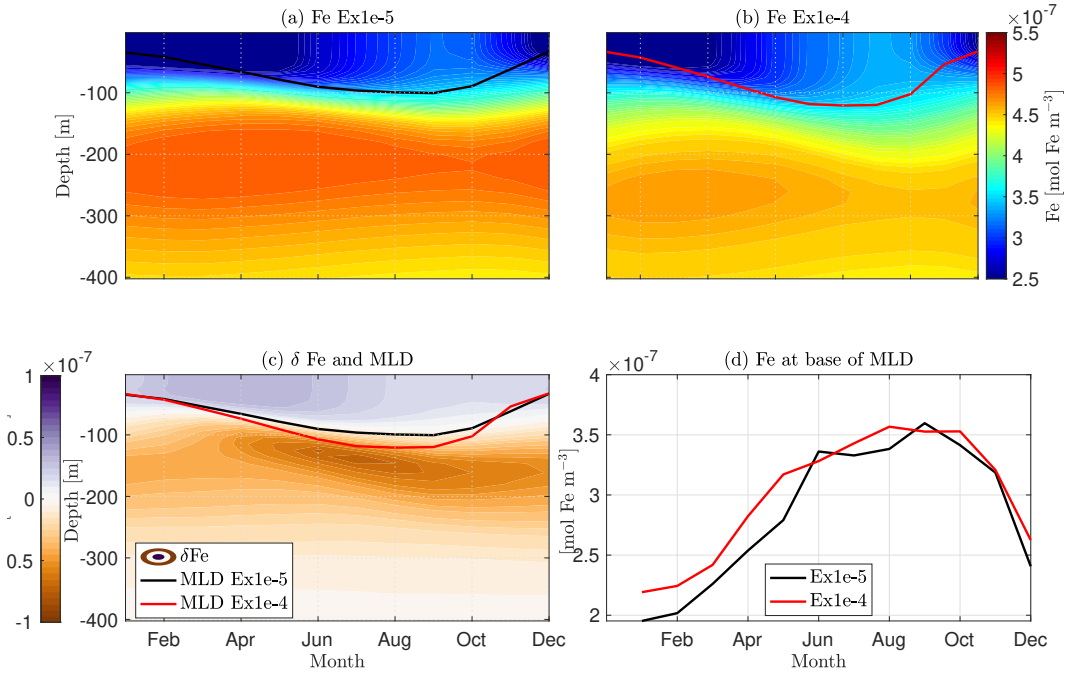

Figure 6. a) Seasonal cycle of Fe concentration and mixed layer depth in Ex1e-5. b) Seasonal cycle of Fe concentration and MLD in Ex1e-4. c) Seasonal cycle of change in Fe concentration (Ex1e-4 - Ex1e-5) and the MLD of Ex1e-4 (red line) and Ex1e-5 (black line). d) Seasonal cycle showing Fe concentration at the base of the mixed layer for Ex1e-5 (black line) and Ex1e-4 (red line) . All plots shown are the mean profiles from between 130°W and 150°W and -55°S to -50°S

can increase or decrease biomass depending on regional subtleties. A reduction in sea ice cover can decrease phytoplankton biomass by increasing wind stress action on the ocean, deepening the MLD, and decreasing light availability. Conversely, increased fresh water input during the spring melt seasons can also increase stratification, helping to shoal the MLD, as is observed in the shallowed MLD along the icesheet edge in Ex1e-4 in September (Fig.3d), increasing light availability. Light availability is further increased due to less reflection with a reduced ice cover. Fe can also be supplied by ice-sheet melt, though this is not represented in B-SOSE. These effects, as well as the strong increase in surface water temperatures are all contributors to the increased biomass when vertical mixing is enhanced. Large phytoplankton blooms have been observed using SOCCOM floats at the ice shelf edge during late spring (Uchida et al., 2019), with ice melt during polynya events also observed to cause strong spring phytoplankton blooms (von Berg et al., 2020).

This work suggests that the representation of diapycnal mixing in the SO has a significant control over the rate of biological productivity. Biological productivity varies on time scales as short as one month, predominately due to an increased diapycnal flux of iron to surface waters. Though this work was only carried out over short timescales, it is possible that increased SO biomass could translate to increased export if it occurs in a subduction zone. The SO is estimated to be responsible for 30% of global carbon export (Schlitzer, 2002; Arteaga et al., 2019). Therefore, changes to biological productivity in the SO could be a driver of changes to atmospheric CO_2 on timescales of hundreds to thousands of years (Sarmiento & Toggweiler, 1984). This emphasises the need for climate models to represent the spatio-temporal variability of small scale turbulent mixing via parameterisations, as the strength and variability of the biological carbon pump could be significantly altered. Further work is required to assess whether areas and seasons showing the strongest increases in biomass are key to the formation of long term organic stores of carbon and on productivity further north of the SO.

Acknowledgments

Enter acknowledgments, including your data availability statement, here.

References

Arteaga, L. A., Pahlow, M., Bushinsky, S. M., & Sarmiento, J. L. (2019, 8). Nutrient Controls on Export Production in the Southern Ocean. *Global Biogeochemical Cycles*, *33*(8), 942–956. Retrieved from `https://onlinelibrary.wiley.com/doi/10.1029/2019GB006236` doi: 10.1029/2019GB006236

Boyd, P. W. (2002, 1). The role of iron in the biogeochemistry of the Southern Ocean and equatorial Pacific: A comparison of in situ iron enrichments. *Deep-Sea Research Part II: Topical Studies in Oceanography*, *49*(9-10), 1803–1821. Retrieved from `https://www.sciencedirect.com/science/article/pii/S0967064502000139` doi: 10.1016/S0967-0645(02)00013-9

Boyd, P. W., Doney, S. C., Strzepek, R., Dusenberry, J., Lindsay, K., & Fung, I. (2008, 5). Climate-mediated changes to mixed-layer properties in the Southern Ocean: assessing the phytoplankton response. *Biogeosciences*, *5*(3), 847–864. Retrieved from `https://bg.copernicus.org/articles/5/847/2008/` doi: 10.5194/bg-5-847-2008

Boyd, P. W. e. a. (2000). A mesoscale phytoplankton bloom in the polar Southern Ocean stimulated by iron fertilization. (0ther articles in the same issue p. 685, 730. *Nature 407: 695-702*.

Cimoli, L., Stegner, A., & Roullet, G. (2017). Meanders and eddy formation by a buoyant coastal current flowing over a sloping topography. *Ocean Science*. doi: 10.5194/os-13-905-2017

Dutkiewicz, S., Sokolov, A., Scott, J., & Stone, P. (2005). A three-dimensional ocean-seaice-carbon cycle model and its coupling to a two- .... *Joint Program on the Science and Policy of Global ....* Retrieved from `http://web.mit.edu/`

405 globalchange/www/MITJPSPGC_Rpt122.pdfhttp://scholar.google.com/
406 scholar?start=100&hl=en&cites=6420488778323234 20#0
407 Fauchereau, N., Tagliabue, A., Bopp, L., & Monteiro, P. M. (2011, 9). The response of
408 phytoplankton biomass to transient mixing events in the Southern Ocean. *Geophysical*
409 *Research Letters*, *38*(17), n/a-n/a. Retrieved from http://doi.wiley.com/10.1029/
410 2011GL048498 doi: 10.1029/2011GL048498
411 Ferrari, R. (2014). *Oceanography: What goes down must come up.* doi: 10.1038/513179a
412 Galbraith, E. D., Gnanadesikan, A., Dunne, J. P., & Hiscock, M. R. (2010). Regional impacts
413 of iron-light colimitation in a global biogeochemical model. *Biogeosciences*, *7*(3),
414 1043–1064. Retrieved from www.biogeosciences.net/7/1043/2010/ doi: 10.5194/
415 bg-7-1043-2010
416 Ganachaud, A., & Wunsch, C. (2000, 11). Improved estimates of global ocean circulation,
417 heat transport and mixing from hydrographic data. *Nature*, *408*(6811), 453–457. Re-
418 trieved from http://www.nature.com/articles/35044048 doi: 10.1038/35044048
419 Garabato, A. C., Stevens, D. P., Watson, A. J., & Roether, W. (2007). Short-circuiting of
420 the overturning circulation in the Antarctic Circumpolar Current. *Nature*, *447*(7141),
421 194–197. Retrieved from https://www.nature.com/articles/nature05832.pdf
422 doi: 10.1038/nature05832
423 Gaspar, P., Grégoris, Y., & Lefevre, J.-M. (1990, 9). A simple eddy kinetic en-
424 ergy model for simulations of the oceanic vertical mixing: Tests at station Papa
425 and long-term upper ocean study site. *Journal of Geophysical Research*, *95*(C9),
426 16179. Retrieved from http://doi.wiley.com/10.1029/JC095iC09p16179 doi:
427 10.1029/JC095iC09p16179
428 Gnanadesikan, A., Dunne, J. P., Key, R. M., Matsumoto, K., Sarmiento, J. L., Slater, R. D.,
429 & Swathi, P. S. (2004). Oceanic ventilation and biogeochemical cycling: Under-
430 standing the physical mechanisms that produce realistic distributions of tracers and
431 productivity. *Global Biogeochemical Cycles*, *18*(4), 1–17. Retrieved from https://
432 agupubs.onlinelibrary.wiley.com/doi/pdf/10.1029/2003GB002097https://
433 pdfs.semanticscholar.org/09bf/eb7e7728fb8ad30f253e13e72adf20992330.pdf
434 doi: 10.1029/2003GB002097
435 Gruber, N., Gloor, M., Mikaloff Fletcher, S. E., Doney, S. C., Dutkiewicz, S., Follows, M. J.,
436 ... Takahashi, T. (2009, 3). Oceanic sources, sinks, and transport of atmospheric
437 CO ¡sub¿2¡/sub¿. *Global Biogeochemical Cycles*, *23*(1), n/a-n/a. Retrieved from
438 http://doi.wiley.com/10.1029/2008GB003349 doi: 10.1029/2008GB003349
439 Ito, T., & Follows, M. J. (2005). Preformed phosphate, soft tissue pump and atmospheric
440 CO 2. *Journal of Marine Research*. Retrieved from http://ocean.mit.edu/~mick/
441 Papers/ItoFollows-preformed-JMR2005.pdf doi: 10.1357/0022240054663231
442 Lefèvre, N., & Watson, A. J. (1999, 9). Modeling the geochemical cycle of iron in the
443 oceans and its impact on atmospheric CO ¡sub¿2¡/sub¿ concentrations. *Global Biogeo-*
444 *chemical Cycles*, *13*(3), 727–736. Retrieved from http://doi.wiley.com/10.1029/
445 1999GB900034 doi: 10.1029/1999GB900034
446 Llort, J., Lévy, M., Sallée, J. B., & Tagliabue, A. (2019, 3). Nonmonotonic Re-
447 sponse of Primary Production and Export to Changes in Mixed-Layer Depth in
448 the Southern Ocean. *Geophysical Research Letters*, *46*(6), 3368–3377. Retrieved
449 from https://onlinelibrary.wiley.com/doi/abs/10.1029/2018GL081788 doi:
450 10.1029/2018GL081788
451 Longhurst, A. R. (1991, 12). Role of the marine biosphere in the global carbon cycle.
452 *Limnology and Oceanography*, *36*(8), 1507–1526. Retrieved from http://doi.wiley
453 .com/10.4319/lo.1991.36.8.1507 doi: 10.4319/lo.1991.36.8.1507
454 Lumpkin, R., & Speer, K. (2007). Global ocean meridional overturning. *Journal of Physical*
455 *Oceanography*, *37*(10), 2550–2562. Retrieved from https://journals.ametsoc.org/
456 doi/pdf/10.1175/JPO3130.1 doi: 10.1175/JPO3130.1
457 Manizza, M., Quéré, C. L., Watson, A. J., & Buitenhuis, E. T. (2005, 3). Bio-optical feed-
458 backs among phytoplankton, upper ocean physics and sea-ice in a global model. *Geo-*
459 *physical Research Letters*, *32*(5), L05603. Retrieved from http://doi.wiley.com/

10.1029/2004GL020778 doi: 10.1029/2004GL020778

Mashayek, A., Ferrari, R., Merrifield, S., Ledwell, J. R., St Laurent, L., & Garabato, A. N. (2017). Topographic enhancement of vertical turbulent mixing in the Southern Ocean. *Nature Communications*, *8*. Retrieved from http://dimes.ucsd.edu/en/ doi: 10.1038/ncomms14197

Munk, W. H. (1966, 8). Abyssal recipes. *Deep-Sea Research and Oceanographic Abstracts*, *13*(4), 707–730. Retrieved from https://linkinghub.elsevier.com/retrieve/pii/0011747166906024 doi: 10.1016/0011-7471(66)90602-4

Palter, J. B., Sarmiento, J. L., Gnanadesikan, A., Simeon, J., & Slater, R. D. (2010). Fueling export production: Nutrient return pathways from the deep ocean and their dependence on the Meridional Overturning Circulation. *Biogeosciences*. doi: 10.5194/bg-7-3549-2010

Parekh, P., Follows, M. J., & Boyle, E. A. (2005, 6). Decoupling of iron and phosphate in the global ocean. *Global Biogeochemical Cycles*, *19*(2), 1–16. Retrieved from http://doi.wiley.com/10.1029/2004GB002280 doi: 10.1029/2004GB002280

Sallée, J. B., Pellichero, V., Akhoudas, C., Pauthenet, E., Vignes, L., Schmidtko, S., ... Kuusela, M. (2021). Summertime increases in upper-ocean stratification and mixed-layer depth. *Nature*, *591*(7851), 592–598. Retrieved from https://doi.org/10.1038/s41586-021-03303-x doi: 10.1038/s41586-021-03303-x

Sallée, J. B., Speer, K. G., & Rintoul, S. R. (2010, 4). Zonally asymmetric response of the Southern Ocean mixed-layer depth to the Southern Annular Mode. *Nature Geoscience*, *3*(4), 273–279. Retrieved from http://www.nature.com/articles/ngeo812 doi: 10.1038/ngeo812

Sarmiento, J. L., Gruber, N., Brzezinski, M. A., & Dunne, J. P. (2004, 1). High-latitude controls of thermocline nutrients and low latitude biological productivity. *Nature*, *427*(6969), 56–60. Retrieved from http://www.nature.com/articles/nature02127 doi: 10.1038/nature02127

Sarmiento, J. L., & Toggweiler, J. R. (1984, 4). A new model for the role of the oceans in determining atmospheric PCO 2. *Nature*, *308*(5960), 621–624. Retrieved from http://www.nature.com/articles/308621a0 doi: 10.1038/308621a0

Schlitzer, R. (2002). Carbon export fluxes in the Southern Ocean: Results from inverse modeling and comparison with satellite-based estimates. *Deep-Sea Research Part II: Topical Studies in Oceanography*. doi: 10.1016/S0967-0645(02)00004-8

Schmittner, A., Oschlies, A., Giraud, X., Eby, M., & Simmons, H. L. (2005, 9). A global model of the marine ecosystem for long-term simulations: Sensitivity to ocean mixing, buoyancy forcing, particle sinking, and dissolved organic matter cycling. *Global Biogeochemical Cycles*, *19*(3), 1–17. Retrieved from http://doi.wiley.com/10.1029/2004GB002283 doi: 10.1029/2004GB002283

Sigman, D. M., Hain, M. P., & Haug, G. H. (2010). *The polar ocean and glacial cycles in atmospheric CO2 concentration* (Vol. 466) (No. 7302). doi: 10.1038/nature09149

Swart, S., Thomalla, S. J., & Monteiro, P. M. (2015, 7). The seasonal cycle of mixed layer dynamics and phytoplankton biomass in the Sub-Antarctic Zone: A high-resolution glider experiment. *Journal of Marine Systems*, *147*, 103–115. Retrieved from https://www.sciencedirect.com/science/article/abs/pii/S0924796314001535 doi: 10.1016/j.jmarsys.2014.06.002

Swierczek, S., Mazloff, M. R., Morzfeld, M., & Russell, J. L. (2021, 7). The effect of resolution on vertical heat and carbon transports in a regional ocean circulation model of the Argentine Basin. *Journal of Geophysical Research: Oceans*, *126*(7), e2021JC017235. Retrieved from https://onlinelibrary.wiley.com/doi/10.1029/2021JC017235 doi: 10.1029/2021jc017235

Tagliabue, A., Williams, R. G., Rogan, N., Achterberg, E. P., & Boyd, P. W. (2014, 10). A ventilation-based framework to explain the regeneration-scavenging balance of iron in the ocean. *Geophysical Research Letters*, *41*(20), 7227–7236. Retrieved from http://doi.wiley.com/10.1002/2014GL061066 doi: 10.1002/2014GL061066

Takahashi, T., Sutherland, S. C., Wanninkhof, R., Sweeney, C., Feely, R. A., Chipman,

D. W., ... de Baar, H. J. (2009, 4). Climatological mean and decadal change in surface ocean pCO2, and net sea–air CO2 flux over the global oceans. *Deep Sea Research Part II: Topical Studies in Oceanography*, *56*(8-10), 554–577. Retrieved from https://linkinghub.elsevier.com/retrieve/pii/S0967064508004311 doi: 10.1016/j.dsr2.2008.12.009

Talley, L. D. (2013). Closure of the global overturning circulation through the Indian, Pacific, and southern oceans. *Oceanography*, *26*(1), 80–97. Retrieved from http://dx.doi.org/10.5670/oceanog.2013.07 doi: 10.5670/oceanog.2013.07

Talley, L. D., Reid, J. L., & Robbins, P. E. (2003, 10). Data-Based Meridional Overturning Streamfunctions for the Global Ocean. *Journal of Climate*, *16*(19), 3213–3226. Retrieved from http://journals.ametsoc.org/doi/10.1175/1520-0442(2003)016<3213:DMOSFT>2.0.CO;2 doi: 10.1175/1520-0442(2003)016⟨3213:DMOSFT⟩2.0.CO;2

Uchida, T., Balwada, D., Abernathey, R., Prend, C. J., Boss, E., & Gille, S. T. (2019, 11). Southern Ocean Phytoplankton Blooms Observed by Biogeochemical Floats. *Journal of Geophysical Research: Oceans*, *124*(11), 7328–7343. Retrieved from https://onlinelibrary.wiley.com/doi/10.1029/2019JC015355 doi: 10.1029/2019JC015355

Venables, H., & Moore, C. M. (2010, 2). Phytoplankton and light limitation in the Southern Ocean: Learning from high-nutrient, high-chlorophyll areas. *Journal of Geophysical Research*, *115*(C2), C02015. Retrieved from http://doi.wiley.com/10.1029/2009JC005361 doi: 10.1029/2009jc005361

Verdy, A., & Mazloff, M. R. (2017). A data assimilating model for estimating Southern Ocean biogeochemistry. *Journal of Geophysical Research: Oceans*, *122*(9), 6968–6988. Retrieved from http://hycom.org doi: 10.1002/2016JC012650

von Berg, L., Prend, C. J., Campbell, E. C., Mazloff, M. R., Talley, L. D., & Gille, S. T. (2020, 6). Weddell Sea Phytoplankton Blooms Modulated by Sea Ice Variability and Polynya Formation. *Geophysical Research Letters*, *47*(11). doi: 10.1029/2020GL087954

Waterhouse, A. F., Mackinnon, J. A., Nash, J. D., Alford, M. H., Kunze, E., Simmons, H. L., ... Lee, C. M. (2014). Global patterns of diapycnal mixing from measurements of the turbulent dissipation rate. *Journal of Physical Oceanography*. doi: 10.1175/JPO-D-13-0104.1

Watson, A. J., Ledwell, J. R., Messias, M. J., King, B. A., Mackay, N., Meredith, M. P., ... Naveira Garabato, A. C. (2013, 9). Rapid cross-density ocean mixing at mid-depths in the Drake Passage measured by tracer release. *Nature*, *501*(7467), 408–411. Retrieved from http://www.nature.com/articles/nature12432 doi: 10.1038/nature12432

Williams, R. G., & Follows, M. J. (2011). *Ocean Dynamics and the Carbon Cycle*. Cambridge: Cambridge University Press. Retrieved from http://ebooks.cambridge.org/ref/id/CBO9780511977817 doi: 10.1017/CBO9780511977817

Yoon, J.-E., Yoo, K.-C., Macdonald, A. M., Yoon, H.-I., Park, K.-T., Yang, E. J., ... Kim, I.-N. (2018, 10). Reviews and syntheses: Ocean iron fertilization experiments – past, present, and future looking to a future Korean Iron Fertilization Experiment in the Southern Ocean (KIFES) project. *Biogeosciences*, *15*(19), 5847–5889. Retrieved from https://www.biogeosciences.net/15/5847/2018/ doi: 10.5194/bg-15-5847-2018